A zebrafish model of developmental joint dysplasia: Manipulating the larval mechanical environment to drive the malformation and recovery of joint shape.

Short title – Zebrafish joint shape recovery

Authors

Karen A Roddy[1], Roddy EH Skinner[1], Lucy H Brunt[1], Erika Kague[1], Stephen Cross[1], Emily J Rayfield[2], Chrissy L Hammond[1]*

1. School of Physiology, Pharmacology and Neuroscience, University of Bristol, BS8 1TD, U.K.

2. School of Earth Sciences, University of Bristol, BS8 1TD, U.K.

* Email: Chrissy.Hammond@bristol.ac.uk

Abstract

Developmental dysplasia of the hip (DDH), a malformation of the acetabulum, is a frequent cause of early onset osteoarthritis. The disease encompasses a spectrum of severities, some of which are more amenable to treatment. Embryonic immobilisation significantly impairs the development of joint shape however the impact of this malformation to the function and growth of the joint in the short to medium term is unclear. We developed a novel model of developmental joint dysplasia using the zebrafish jaw joint to identify the mechanisms regulating cellular plasticity and ability to recover joint shape and function. Larval zebrafish were immobilised either pharmacologically or using targeted ablation of jaw muscles to induce an altered joint shape. Following restoration of muscle activity we dynamically monitored the joint shape and function in individuals at cellular resolution impossible in other vertebrate species. Reflecting the variability of the human condition we found a proportion of joints will recover both their shape and function, while others will not; despite coming from a genetically homogenous population. This allowed us to study what controls likelihood of recovery; we identified a number of cellular changes that predict likelihood of functional recovery, including position of precursor cells, and specific patterns of proliferation, migration and differentiation in joints and associated connective tissues. These factors together predict recovery better than severity of malformation alone. Using Finite Element Analysis we studied the mechanics of joints representative of ones that recover and those that fail to identify differences in patterns of strain that could explain the cellular behaviours that underpin likelihood of recovery. Thus, this model would enable the study of the short to long term impact of altered joint shape on function and could help to identify the changes that render an individual more receptive to treatment and therefore may potentially be indicative of long term joint health.

Introduction

The complex shape of a synovial joint is a vital component of its function; governing its range of motion and capacity to efficiently transmit load. Congenital joint shape defects, such as developmental dysplasia of the hip (DDH) increase an individual's risk of osteoarthritis (OA) even if treated successfully; although some subtle forms of DDH can resolve spontaneously [1]. DDH, caused by a shallow acetabulum leading to a joint prone to subluxation is associated with factors that constrain foetal and postnatal movement including breech presentation and swaddling [2]. DDH has a dramatic impact on the hip joint but more subtle variations in joint shape have been associated with increased risk of developing osteoarthritis [3,4]. Thus, joint shape is an important regulator of joint fitness. Current treatment for DDH using a Pavlic harness relies on postnatal remodelling and growth to modify the shape of growing joint, however, success is linked to early treatment and failure to surgical intervention [1]. The mechanisms through which these abnormal joint shapes are corrected, and the factors governing the optimal window for treatment remain unclear.

Mechanoregulatory signals generated by muscle contraction are vital to the development of its characteristic 3D structure [5-9] and have been suggested as primary driver of DDH development [10]. Studies in the chick [6,11,12], mouse [13-15] and zebrafish [5,15,16] have shown that loss of muscle activity leads to malformed joints lacking features such as ligaments, articular cartilage, meniscus and articular processes. Gradients of shear, tension and compression are created during muscle contractions and cells are differentially responsive to these varying mechanical signals altering their cell behaviour or differentiation in response to the changing mechanical force [17-19]. Mechanical stimulus is also a major modifier of disease progression in OA. Immobilising murine knee joints after surgical destabilisation, reduces expression of OA associated genes and protects these joints from degeneration [20] and also slows tissue damage in patients with established OA [21,22]. However, immobilisation can also drive the degeneration of healthy cartilage [23]. Thus, mechanical stimulus wrongly applied can be detrimental to joint health. How aberrant

mechanical stimuli, generated by the movement of a malformed joint might be integrated into the regulatory framework governing postnatal growth in order to achieve joint recovery is poorly understood.

Various models of DDH exist; including spontaneous canine models [24,25], cast/swaddling models in rats and rabbits [26,27] and foetal immobilisation [10]. Canine and cast/swaddling models do not recapitulate the initial development of DDH as the hip is normal at birth. The chick immobilisation model can induce a shallow acetabulum however joint degeneration has not been confirmed. Here we present a zebrafish model that facilitates the study of the early developmental steps leading to a subluxed joint and the testing of factors underpinning likelihood of recovery. Zebrafish develop externally making them tractable for drug treatment or laser surgery. Zebrafish have synovial joints and have been demonstrated to develop phenotypes resembling osteoarthritis as they age [28,29]. Most importantly the availability of transgenic lines labelling the developing skeleton enables studies of cell behaviour in live larvae [39}. We hypothesise that restoration of movement, following immobilisation, drives morphogenetic changes in the zebrafish jaw and joint remodelling. To test this, we induced jaw joint malformation using a period of pharmacological immobilisation [5] or by muscle ablation, then allowed movement to resume and tracked the changing jaw shape, cell behaviour and differentiation. Laser ablation has been used to study repair mechanisms after injury [30] and was used here to sever the adductor mandibularis. We show that immobilised larvae that recover have a significantly different joint shape to those that fail to recover; and they successfully remodel the joint and associated tissues including the ligament and enthesis. We also demonstrate that recovery potential is underpinned, in part, by changes to cell orientation, migration and proliferation. Using finite element analysis to explore the mechanoregulatory environment experienced by recovering and subluxed larvae we identify differences.in patterns of strain that could explain the cellular behaviours that underpin likelihood of recovery.

Results

Resumption of movement following immobilisation leads to changes in jaw placement.

The anaesthetic MS222 (tricaine) induces flaccid paralysis in zebrafish and has been shown to lead to malformation of the jaw joint and changes to joint cell behaviour [5,15,16]. To determine the capacity of these malformed joints to recover functionality larvae were treated with MS222 for 48hrs from 3-5dpf then allowed to resume movement. To rule out secondary drug effects and to investigate the impact of targeted change to jaw mechanics we also developed a model in which we bilaterally ablated the adductor mandibularis, which is responsible for jaw closure, using a laser. Following ablation, muscle regrowth was visible by 1 day post ablation (dpa) and muscle fibres reconnected the elements and were contractile by 2dpa (at 5dpf) (S1 Fig).

Following either anaesthesia or muscle ablation the jaw joint was subluxed in all larvae such that it was rendered unable to close (S1-3 Video) at 5dpf (Fig 1B-C, 1-2). Underlying this loss of function was a significant change to the shape of the MC and jaw joint which lacked the complementary surfaces of control joints (Fig 1A-C, 3-4). Rather, the MC overlapped the palatoquadrate on the medial side of the joint (Fig 1A-C, 3-4, arrowhead). Anaesthesia and muscle ablation also caused flattening and thickening of the anterior tip of the MC, close to the mandibular symphysis (Fig 1B3, C3, double headed arrow). Following removal from MS222, treated larvae moved their jaws significantly more frequently than control larvae (Fig 1D), potentially due to mild hypoxia. Although all AM-ablated larvae resumed movement, indicating regeneration, they had significantly fewer jaw movements than controls (Fig 1D) (S1 Fig), likely due to the reduced contractile ability of the regenerating fibres at the stages observed.

By 7dpf the majority of immobilised and of ablated larvae recovered from the subluxed position, such that they could now fully close the mouth (Fig 1E-I, 1,2 arrows). Larvae with a

120 "recovered" jaw position (Fig 1F, H) displayed complementary joint surfaces, and an
121 appropriately positioned retro-articular process (RAP) (Fig 1F,H), resembling the
122 appearance of unmanipulated controls. The remaining larvae retained their subluxed jaw
123 position (Fig 1G1-2, I1-2, arrows) with overlapping joint surfaces (Fig 1G3-4, I3-4
124 arrowhead).

125 Severity of joint malformation correlates with timing and duration of anaesthesia treatment
126 [5]. We varied the timing and duration of treatment to determine if these factors also
127 determine ability to recover joint shape and function following resumption of movement. We
128 immobilised zebrafish for 24, 48 or 56 hours from 72 or 96hpf (Fig 1J) and monitored the
129 percentage of larvae that recovered following drug wash out and resumption of muscle
130 activity (Fig 1K). Recovery was significantly affected by the timing of treatment. When
131 movement resumed prior to 4dpf 95% of larvae recovered by 7dpf, a significantly higher
132 percentage than the worst performing treatment group (those larvae immobilised for 56
133 hours) from which only 69 % recovered (Fig 1K). Folllowing ablation 84% of larvae
134 recovered, however, due to low sample number (n=30) these were not included in statistical
135 tests. These results indicate that there is sufficient joint plasticity at 5dpf to enable most
136 larvae to recover functionality, however earlier resumption of movement significantly
137 improves chance of recovery.

138 *Anaesthesia significantly alters the overall shape of the Meckel's cartilage*

139 To investigate the impact of immobilisation and restored movement on MC shape we used
140 geometric morphometric analysis. In addition to immobilised and ablated larvae we included
141 Myod-/- which lack jaw musculature [31] to model continued jaw joint paralysis. Control,
142 Myod-/-, larvae anaesthetised from 3-5dpf and larvae with ablated AM were imaged live at
143 5dpf then each larva re-imaged at 7dpf. At 7dpf immobilised and AM-ablated larvae were
144 classified as "Subluxed" or "Recovered". Outlines of the MC at 5dpf (Fig 2A) were analysed
145 using npManova and between-groups Principal Component Analysis (bgPCA) [16] to
146 quantify how MC shape differs between the groups. Each principal component (PC)

describes a trend in how the shapes within the analysis vary. Thus, similar shapes occupy similar positions along a PC axis while different shapes occupy opposing ends. A shape is described fully by all components as they may be similar in one component but differ in another.

Loss of muscle activity had a significant effect on the shape of the MC at 5dpf. The anaesthetised, ablated and Myod-/- larvae were all significantly different from control larvae (Fig 2B, S1 Table) and occupied different quadrants in PC1 and PC2 of the morphospace relative to control. PC1 accounts for 78.4% of variation in shape, separates the groups based on increasing MC width near the mandibular symphysis and degree of joint overlap (Fig 2D, F). PC2 accounts for 15.5% of the variation and captures the shape of the MC arch; control and Myod mutants are more gently arched than anaesthetised or ablated larvae. Ablated and anaesthetised larvae collocate while Myod mutants are dramatically different to controls. At 5dpf there was no significant difference in shape between larvae that will recover and those that remain subluxed at 7dpf (Fig 2B, D, F S1 Table). As such, MC shape at 5dpf does not reliably predict likelihood of recovery.

Resuming movement had a significant impact on the shape of the larval jaw at 7dpf. PC1 and PC2 accounted for 73.4% and 14.3% of variation between the groups; describing similar trends as at 5dpf (Fig 2E). The shapes of recovered jaws at 7dpf were significantly different from those that remained subluxed (Fig 2C, S2 Table) occupying an intermediate position in the morphospace plot, overlapping both the control and subluxed domains (Fig 2E, G). These data indicate that within a pool of similarly treated larvae a subgroup can recover a functional joint and the resultant recovered shape differs significantly from the shape of those that remain subluxed.

Differences in cell orientation, shape and size precede recovery.

Morphospace analysis highlighted the impact of altered load on mandibular symphysis and jaw joint shape. The differentiation of cells at both sites is affected by loss of muscle activity

[5,15,16]. As chondrocytes mature their appearance changes from small spherical cells to larger ellipsoids [32]. Therefore, chondrocyte differentiation state can be inferred by measuring their size and circularity. A perfect circle has a circularity of 1, with decreasing values for elongated cells. We compared the shape and size of chondrocytes in the anterior MC in control, Myod-/-, anaesthetised and ablated larvae, with the latter two groups subdivided by their status at 7dpf. Cells flanking the mandibular symphysis were outlined and circularity and area calculated for each cell (Fig 3A-J). Due to the small number of AM ablated larvae that remained subluxed all further analysis on AM-ablated larvae were carried out on jaws that were classed as recovered at 7dpf. At 5dpf midline chondrocytes were significantly smaller and rounder in Myod-/- mutants and larvae that remain subluxed than controls and larvae that recover. At 7dpf only chondrocytes in larvae that remain immobile, i.e. Myod-/-, were significantly rounder than control, suggesting that movement drives maturation of this cell population.

Immobility leads to alterations to joint cell orientation and size [5]. To determine whether restoration of normal cell size and orientation is achieved during recovery we measured the chondrocytes located at the joint (Fig 3O-Q, S2 Fig). At 5dpf joint chondrocytes in anaesthetised larvae that will recover were statistically indistinguishable to controls; while chondrocytes in those that failed to recover, Myod-/- and AM-ablated larvae, were significantly smaller than the chondorcytes of controls (Fig 3P). No significant difference in cell size was seen between any of the groups at 7dpf; due to the variability of control cell size (Fig 3Q). Analysis of the orientation of the major axis of joint cells relative to the palatoquadrate surface, revealed significant differences in orientation of cells at 5dpf on both the medial and lateral joint sides in larvae that fail to recover relative to controls, whereas joint cells from larvae that will recover do not differ from controls. By 7dpf the orientation of cells in subluxed treated larvae are no longer significantly different from controls and recovered larvae, whereas Myod-/- larvae, which receive no mechanical input remain significantly different to controls (S2 Fig B, C). This data demonstrates that variation in size

and orientation of cells located at the joint and symphysis at 5dpf are associated with ability to recover; and that reapplication of mechanical stimulus allows cells to reorientate.

Movement drives restored expression of joint associated genes

Loss of muscle activity in amniotes leads to cartilage fusion in the joint territory driven by loss of joint specific markers in favour of the expression of *Collagen 2* (*Col2*) and other cartilage markers [6,12,33]. We used the relationship between *Col2a1*, a marker of mature chondrocytes, and *Sox10*, a marker of neural crest [34] expressed in immature craniofacial chondrocytes and joint precursor cells (Fig 4A), to determine if joint boundaries re-emerge during recovery. At 3dpf cells expressing *Sox10* were seen across the whole joint, with particularly strong expression on the medial side where the RAP forms (Fig 4A 2, 3, 6). At 5 and 7dpf cells in the joint line, tip of the RAP and 2-4 cells flanking the mandibular symphysis express high levels of *Sox10* and much lower levels of *Col2a1* (Fig 4 A4, 5, 7).

To alleviate variation in the intensity of *Sox10* or *Col2a1* due to copy number variation or imaging parameters we extracted the anti-correlation component of the “product of the difference of the mean” (PDM) [35] of the confocal dataset. In 5dpf controls *Sox10* was expressed across the joint line in cells where *Col2a1* was not expressed; these cells were clearly identifiable in the PDM (Fig 4B, arrows). In comparison immobilisation lead to a significant reduction in the size and definition of the joint domain, particularly apparent in Myod mutants (Fig 4B, D). The magnitude of the anti-correlation component, indicative of how different the two channels were, was also significantly reduced in Myod-/- larvae at 5dpf (S3 Fig).

At 7dpf the relative expression of *Sox10* and *Col2a1* remained significantly disrupted in subluxed and Myod-/- larvae (Fig 4C, E), whereas the joint region of recovered larvae and AM-ablated larvae were no longer significantly different to controls (Fig 4E). Thus, larvae capable of recovery reacquire a group of cells with high *Sox10* low *Col2a1*, suggestive of

immaturity/plasticity in the joint, whereas larvae that fail to recover or remain paralysed fail to maintain these joint specific cells.

Recovery is driven by changes to cell proliferation and migration.

We hypothesised that proliferation and/or migration of these *Sox10* high *Col2* low cells might drive joint recovery. Cell proliferation following the resumption of movement was measured by treating larvae with BrdU from 5-7dpf, at which time the larvae were sorted into recovered and subluxed groups, stained immune-fluorescently and quantified (Fig 5C, D). BrdU incorporation was significantly increased, relative to control, on both the medial and lateral side of the joint in subluxed larvae. In contrast, proliferation was only increased on the lateral side of the joint in recovered larvae (Fig 5 D). BrdU+ cells were present in larger numbers in the lateral joint margin (Fig 5A arrowhead) in both groups relative to control.

Cell migration during recovery was assayed by photoconvertion of kaede-expressing cells in zebrafish carrying Tg(Sox10:GAL4-VP16) and Tg(UAS:Kaede) transgenes. Kaede protein is green in its native state but is irreversibly photoconverted to red using UV light. 8-10 cells were photoconverted at 5dpf on either the medial or the lateral side of joints in larvae that were anaesthetised and in controls. These larvae were then reimaged at 7dpf to track the behaviour of the photoconverted cells. The spread of cells across the joint was calculated as the change in the area of the photoconverted domain (Fig 5E, F), measured from max projections between 5 and 7dpf (Fig 5B, red outline). Cellular migration was significantly increased on the lateral side of recovered but not subluxed larvae (Fig 5E, F). There was also evidence of cellular reorientation on the lateral side of recovered joints that was not apparent in subluxed larvae (Fig 5B arrowhead). In comparison, no changes to cellular orientation or spread of photoconverted cells were detected on the medial side. This data indicates that cells at the joint retain the capacity to adapt to the mechanical environment and sculpt the joint by modifying regional patterns of cell migration and proliferation.

Joint associated structures such as ligaments and their insertions are restored in recovered larvae.

Immobilisation during development has been shown to have a significant impact on the structure of joint associated tissues such as ligaments and their attachments [6,11,36]. The RAP, the insertion site of the interoperculomandibular ligament (IOM) is significantly impacted by loss of mechanical load (Fig 1,2) [5,16]. C*ol10a1:citrine (ColX)* was expressed by osteoblasts in the ligament entheses (Fig 6A ,E) [37] and at a lower level throughout the IOM ligament (Fig 6A, E). It was used to assess the impact of immobilisation (Fig 6 A-D) and recovery (Fig 6E-I) on osteoblast number in the RAP and ligament width. Immobilisation caused a significant reduction in osteoblast number in the RAP at 5dpf (Fig 6C). By 7dpf the number of osteoblasts at the RAP of subluxed, but not recovered larvae, were significantly fewer than controls (Fig 6 E-H).

At 5dpf, the width of the IOM ligament was significantly increased in immobilised larvae reflecting a loss of the tight cohesive structure characteristic of ligaments (Fig 5D). At 7dpf the subluxed cohort remained marginally larger but this was not significant, possibly due to the small sample number (n=4). We verified the recovery of the ligament by comparing the number of ligament cells that incorporated BrdU between 5 and 7dpf in control, subluxed and recovered larvae. Larvae that recover proliferated significantly more between 5 and 7dpf than either control or subluxed larvae. Therefore, larvae that successfully recover a functional shape also repair the degenerative impact of immobilisation on the interzone and joint associated tissues such as ligaments.

Recovery potential is associated with regional differences in the pattern, magnitude and orientation of mechanical stimuli within the jaw

Mechanical forces act as a form of positional information with cells behaving in a regionally specific manner dependent on its mechanical environment. We hypothesised that joint shape, cellular orientation and differentiation could feed into the mechanical environment

276 ,which in turn regulates the cells, producing a feedback loop resulting either in success or in
277 failure. Renewed movement is required for the initiation of shape recovery and may drive the
278 rapid correction seen in recovered larvae. Finite element (FE) models of representative 5dpf
279 control, anaesthetised recovered and subluxed larva were analysed to identify potential
280 differences in the pattern of biophysical stimuli experienced by larvae that recover and those
281 that remain subluxed. The range of motion of the tip of the jaw in control and anaesthetised
282 larvae was 53.3 (+/- 18.4) μm and 57.71(+/- 22.5) μm respectively, which was replicated by
283 the displacement of the FE models during the closure step (Fig 7A-C). The insertion of the
284 IOM (interosseous membrane) ligament at the jaw joint generates a distinct peak in strain,
285 which is located at the tip of the RAP in controls (Fig 7D, J, Fig S6A). This peak correlates
286 with the position of *Col10a1* expressing osteoblasts; which are mechanically responsive and
287 reduced in anaesthetised larvae (Fig 6). The mandibular symphysis is also a site of
288 increased mechanical load in models of 5dpf control and recovered larvae (Fig7, D-E,J-K
289 arrow head) but not the subluxed model. The orientation/direction of the principal strains
290 within a tissue are important regulators of cell orientation. In the MC the orientation of
291 maximum principal strain, as indicated by the direction of the arrows (Fig 7G-I), closely
292 follows the curvature of the cartilage with a distinct peak at symphysis. Thus cells within the
293 MC are orientated perpendicular to these strains. While the magnitude of the loads are
294 reduced, relative to control, it is still possible to identify a distinct peak at the symphysis in
295 the model of recovery which is absent in the subluxed (Fig 7I).

296 We identified distinct differences in the regional behaviour of cells between larvae that
297 remain subluxed and those that successfully recover. FE modelling has been shown to
298 predict changes to joint shape and cellular behaviour in the developing jaw joint [5]. We used
299 the FE models to identify if larvae that recover also exhibit distinctly different patterns of
300 biophysical stimuli. In controls, the medial side of the joint is highly loaded (Fig 7D, J, black
301 arrowhead). Recovery is generated by a specific pattern of cell proliferation and migration
302 that varies medial-laterally. In joints that recover there is a significant increase in both

303 proliferation and migration on the lateral side of recovering joints that is absent from those
304 that remain subluxed. To determine if the magnitudes and pattern of loading differed
305 between regions of the model we extracted the absolute maximum principal strain for 10
306 nodes on the medial and lateral side of the joint (Fig 7M) and graphed the results (Fig 7N).
307 In all three models the medial side experiences variable but negative absolute maximum
308 strain indicating a dynamic compressive environment. In comparison, the lateral side of both
309 control and recovered models oscillates between positive (tensional) and negative
310 (compressive) strain while the subluxed surface remains under a lower magnitude negative
311 (compressive) strain.

312

313 **Discussion**

314 Here, we present a novel zebrafish model of developmental joint dysplasia; characterising
315 the cellular mechanisms underpinning the recovery of joint function in malformed joints.
316 Immobilised joints lack the complex interlocking joint shape characteristic of synovial joints,
317 which maintain joint position and range of motion, therefore recapitulating many of the
318 features of DDH [8]. Here we demonstrate that the resumption of movement in immobilised
319 zebrafish joints can be used to examine the impact of suboptimal joint shape on joint health,
320 raising the prospect of following manipulated joints throughout the life of the individual.

321 The zebrafish jaw joint, between the MC and Palatoquadrate, was the focus of this study.
322 This joint is synovial and can develop osteoarthritis [38] and has all the key features of
323 mammalian skeleton including articular cartilage, joint cavity, synovium, tendon and
324 ligaments [39,40]. The zebrafish also has a growing array of genetic tools [41] and is
325 amenable to live imaging making it ideal for longitudinal studies. Tricaine immobilisation
326 alters the shape of the jaw joint and MC by altering cell differentiation and proliferation [5,15]
327 and is similar to the method used in the chick model of DDH [10]. Laser muscle ablation
328 induced a similarly malformed jaw joint without the systemic issues associated with drug

329 treatments. We found a significant proportion of both the anaesthetised and ablated larvae
330 could recover a normal jaw position and approximately normal joint shape while those that
331 fail to recover remain subluxed and have a significantly different jaw shape, reflecting the
332 variability seen in human cases of joint dysplasia.

333 DDH symptoms can range from a mild joint laxity that can resolve itself, up to full subluxation
334 requiring reduction. Prognosis is correlated with severity of the malformation of the
335 acetabulum and age of treatment [1]. We hypothesised, that within a similarly treated group,
336 jaw joint shape would be an indicator of recovery. However, morphometric analysis indicated
337 that the shape of the MC at 5dpf was a relatively poor indicator of likelihood of recovery. As
338 a simplified 2D analysis was performed, it is possible that 3D aspects of the shape that might
339 influence recovery were not captured by the analysis. The relationship between the shape
340 and position of the palatoquadrate surface relative to the MC could play a substantial role in
341 recovery and wasn't included in the morphometric analysis.

342 While shape alone could not predict which larvae would recover, chondrocyte behaviours at
343 the mandibular symphysis and joint could. The orientation of cells in the joint is significantly
344 disrupted by immobilisation [5]. At 5dpf, cells in the mandibular symphysis and jaw joint of
345 larvae that remain subluxed were rounder and less differentiated than those that recover.
346 Interestingly, by 7dpf cell orientation is corrected in all samples bar the Myod mutants. The
347 larval response to immobilisation and recovery is a spectrum determined by differences in
348 cell behaviour.

349 Embryonic immobilisation is associated with loss of the articular surfaces, joint fusion and
350 the degeneration of structures such as meniscus and patella [33]. 5dpf immobilised larvae
351 lost the definition of the interzone, which gives rise to the articular cartilage [42]. By 7dpf the
352 anti-correlative relationship between *Sox10* and *Col2a1* expression in the interzone of
353 recovered larva was redefined but remained abnormal in joints that fail to recover (subluxed
354 and Myod mutants). The development of ligaments [6,33] and their insertion sites (Entheses)
355 are particularly vulnerable to loss of mechanical stimulus [43]. In immobilised and ablated

larvae at 5dpf the interoperculomandibular ligament was wider and looser and ossification at the entheses was significantly reduced. By 7dpf recovery ameliorated this impact significantly. Thus, movement corrects not only the shape of the joint but also drives the recovery of vital joint associated structures.

Skeletal morphogenesis requires preferential regional growth, a feature lost during immobilisation. It is achieved by the local moderation of cell migration, proliferation, cell shape and matrix synthesis [33]. Cellular reorientation and shape change are a feature of recovery however immobilisation has been shown to alter patterns of cell proliferation [7,44]. BrdU incorporation and Kaede photoconversion identified a specific pattern of cell proliferation, migration and growth on the lateral side of the joint that was only present in larvae that recover. These local differences in cell behaviour may be driven by specific biomechanical differences between recovered and subluxed larvae.

We developed Finite Element (FE) models based on 3D confocal datasets of control and anaesthetised larvae at 5dpf. The two chosen anaesthetised larvae were representative examples of those that recover and those that remain subluxed. We identified variations between the mechanical stimuli experienced by these anaesthetised larvae, which may in turn drive the restoration of normal joint shape and function. FE results suggest that cells in the Meckel's cartilage orientate themselves perpendicular to the main direction of strain and that this signal is stronger in larvae that successfully recover. This is in keeping with reports that cells align nearly perpendicular to dynamically varying stresses [45]. The mechanoregulation of chondro-progenitor and chondryocyte proliferation and biosynthesis has been extensively studied in a variety of culture system including explants and monolayer in response to a wide range of mechanical stimuli including compression, tension, hydrostatic pressure and fluid flow [46]. The response of cells to a particular load is dependent on the type of load, its mode of application i.e static or cyclic and the magnitude of this load. Cyclical loading of chondrocytes cultured in alginate beads had a positive effect on chondrocyte metabolism increasing cartilage matrix synthesis while static load was

383 degenerative[47]. Cyclical loading impacts the differentiation of cells, increasing Indian
384 hedgehog expression and stimulating chondrocyte proliferation[19]. Stretch also stimulated
385 the proliferation of immature chondrocytes, but not that of hypertrophic chondrocytes [48].
386 Ultimately load appears to differentially regulate the behaviour of cells[18]. Thus
387 morphogenesis is regulated through a combination of intrinsic regulatory signals produced
388 by the tissue itself e.g. Wnt or Bmp signalling, and extrinsic signals produced by mechanical
389 stimuli. These extrinsic stimuli will in turn alter the expression of intrinsic regulators creating
390 a vicious circle of degeneration amplifying the original malformations. Thus the difference
391 between success and failure may be initially quite minor but could be exacerbated by this
392 “intrinsic-extrinsic” feedback loop. It also demonstrates that successful recovery is very
393 dependent on the individual, their specific cellular orientation, joint shape and mechanical
394 environment. This is corroborated by the long term prognosis of DDH which even after
395 treatment is variable[49].

396 It is possible that higher vertebrates, which lack the regenerative capacity of zebrafish [50],
397 would not respond as dramatically to the resumption of movement, though even in humans
398 cases of DDH can resolve spontaneously with no intervention [1]. As skeletal plasticity is
399 preserved in higher vertebrates we believe the zebrafish model could provide useful insight
400 into the mechanism regulating this plasticity. Using either anaesthesia or muscle ablation it
401 will be possible to target specific windows of plasticity during joint development and identify
402 what processes are disrupted and ultimately determine how some larvae are better
403 positioned for recovery, in the hope of identifying why the prognosis from some DDH
404 patients is so severe.

405 **Materials and Methods**

406 **Zebrafish husbandry and lines.**

407 Zebrafish were housed as previously described [51]. Animal experiments were approved by
408 Bristol University animal ethics committee and the UK Home Office. All transgenic and

409 mutant lines have been previously described: TgBAC(*col2a1a:mCherry*)^{hu5910} [52]; Myod^{fh261}
410 [31]; *Tg(-4725sox10:GFP)*^{ba4} [53]; *symhc:EGFP* [54]; Tg(*Sox10:Gal4-VP16*) [55];
411 Tg(UAS:Kaede) [56]; TgBAC(col10a1a:Citrine)^{hu7050} [57]. Sample numbers used are listed in
412 supplementary S 3 Table.

413 **Pharmacological treatment and imaging**

414 Fish were treated for 24 hours beginning 72 hours post fertilisation (hpf) and 96hpf, 48 hrs
415 from 72hpf, or 56 hours from 72hpf (Fig 1E) with 0.1mg/ml MS222 (Tricaine
416 methanesulfonate)(Sigma), diluted in Danieau's buffer refreshed twice daily. Jaw position
417 was assessed daily between 5 and 7dpf (Fig. 1C) and the percentage recovery calculated
418 from at least 4 plates of 30 larvae. Tracked cohorts were imaged on 5 and 7dpf.

419 **Live imaging**

420 Larvae were sedated, embedded ventrally in 0.5% LMP agarose (Sigma) and fluorescence
421 visualised on a Leica SP8 system using a 10x objective. After imaging larvae recovered in
422 fresh Danieau's buffer.

423 **Muscle Ablation**

424 The Tg(*smyhc:EGFP*) transgenic line was used to visualise muscle position. Anaesthetised
425 3dpf larvae were mounted ventrally in 0.2% LMP agarose in Danieau's and adductor
426 mandibulae (AM) muscles bilaterally ablated with a 440nm nitrogen Micropoint laser
427 connected to a Zeiss Axioplan microscope. Ablation success was confirmed by imaging after
428 ablation. As *smyhc:eGFP* is expressed in slow fibres, the efficacy of laser ablation was
429 verified in 3dpf fixed larvae using fluorescent immunohistochemistry [58] against GFP
430 (ab13970 abcam, 1:200) and skeletal myosin (A4.1025 DSHB, 1:200) (S4 Fig).

431 **Jaw movement movies**

Movies were taken as previously described [5]. Larvae were imaged at 30msec per frame for 500 frames and the number of mouth movements and jaw displacement was recorded. Results were analysed by Anova (SPSS).

Analysis of shape variation

Changes to the Meckel's cartilage (MC) shape were quantified using two-dimensional (2D) geometric morphometrics [16]. Outlines of the MC of 5dpf and 7dpf controls, anaesthetised and ablated larva were digitised and analysed by non-parametric MANOVA (npManova) and between-groups Principal Components Analysis (bgPCA). The anaesthetised and ablated larvae were subdivided by the functional position of their jaw (subluxed or recovered) at 7dpf.

Cell orientation, area and shape

Separate Z-projections of 2-3 consecutive slices were created from *Col2a1* labelled images of the MC through the mandibular symphysis and jaw joint. Cell area and the circularity of a minimum of 10 cells between the insertion points of the intermandibularis anterior muscle were analysed [16]. Cell orientation and area were measured for a minimum of 6 joints per condition at 5 and 7dpf [5]. Chondrocytes were subdivided into those located within 3 cell widths of the medial or lateral side of the joint. Graphs were produced and analysed using PAST [59] and PRISM (Version 7).

***Sox10 Col2a1* colocalisation**

Larvae carrying *Col2a1:mcherry* and *sox10:GFP* transgenes were anaesthetised for 48hrs from 3dpf, allowed to recover, imaged at 5 and 7dpf and processed using a custom MATLAB tool. Stacks were binarised using a threshold to remove background noise. The product of difference from mean (PDM) of each image was calculated [35]. In this data positive values correspond to correlation and negative to anti-correlation between the expression of *Sox10* and *Col2a1*, after each has been normalised by average brightness. The anti-correlation dataset was transformed to a positive image, the joint region selected in 2D and the

458 boundary projected across all slices of the image stack. Within each boundary, pixels above
459 the intensity threshold were fit with an alpha shape [60] yielding a measure of the enclosed
460 volume.

461 **Kaede protein photoconversion**

462 Control and anaesthetised double transgenic Tg(*Sox10:GAL4-VP16*) Tg(UAS:Kaede) larvae
463 were mounted ventrally at 5dpf and 8-10 Kaede expressing cells on the medial or lateral side
464 of the joint were photoconverted [58]. Following photoconversion, larvae were kept
465 individually, reimaged at 7dpf and jaw position assessed. Maximum projections of the red
466 channel were prepared [61] and the area of the photoconverted region was calculated
467 before and after recovery.

468 **BrdU immunostaining**

469 Control and 48hrs anaesthetised larvae were treated with 3mM BrdU (Sigma) diluted in
470 Danieau's solution from 5-7dpf. BrdU incorporation was visualised by immunohistochemistry
471 [58] using mouse anti-BrdU (Sigma, 1:100) and rabbit anti-collagen II (Abcam, 1:200), prior
472 to imaging on confocal SP8. BrdU positive cells within the jaw joint cartilage, were counted
473 and divided into the medial and lateral side of the joint.

474 **Finite Element Modelling**

475 Representative confocal images of 5dpf recovered and subluxed larvae expressing
476 *Col2a1:mcherry* were converted into 3D finite element models for comparison with
477 previously published 5dpf control models using Hypermesh (Version 10, Altair Engineering)
478 [5]. All models had a Young's modulus of 1.1 MPa for the cartilage and 0.75MPa for the
479 interzone and mandibular symphysis, and poisons ratio of 0.25 [as described in 5]. Muscle
480 attachments were added to the FE-models for mouth closure (adductor mandibulae) and
481 opening (protractor hyoideus and intermandibularis) using confocal datasets for reference for
482 attachment sites (Fig S5 A,C,E, O-Q, Table S5). Spring elements were used to simulate the
483 Interoperculomandibular ligament (Fig S5, O-Q, S4 Table) [7]. Anaesthesia impacts the

function of both the muscle and ligaments. In the chick Immobilisation causes to a reduction in muscle size and its ability to transmit forces [62,63]. The magnitudes of the forces applied to the model were therefore adjusted to 75% of the normal estimation [derived from 63]. Immobilisation of the mouse cruciate ligament also reduced its stiffness and peak force[64]. The stiffness of the spring was reduced to 75% (1.3E-0.4 kN/mm). Immobilisation disrupts the definition of the interzone. While a clear interzone could be identified in control and recovered images it was not possible to identify a clear interzone spanning the joint space in the subluxed dataset, therefore the joint was modelled as a fusion with a collar of interzone (Fig S5 O). The geometrically linear models of approximately 2 million tetrahedral elements were imported from into Abaqus FE-software (v6.14 Simulia, Dassault Systèmes), the spring elements were assigned and the model was analysed (v6.10.2 Simulia, Dassault Systèmes).

Acknowledgments

The authors would like to thank the Wolfson Bioimaging Centre, Jen Bright and David Gurevich for their technical advice and support.

.

References

1. Dezateux C, Rosendahl K Developmental dysplasia of the hip. The Lancet 369: 1541-1552.
2. Chan A, McCaul KA, Cundy PJ, Haan EA, Byron-Scott R (1997) Perinatal risk factors for developmental dysplasia of the hip. Archives of Disease in Childhood - Fetal and Neonatal Edition 76: F94-F100.
3. Haverkamp DJ, Schiphof D, Bierma-Zeinstra SM, Weinans H, Waarsing JH (2011) Variation in joint shape of osteoarthritic knees. Arthritis & Rheumatism 63: 3401-3407.
4. Neogi T, Bowes MA, Niu J, De Souza KM, Vincent GR, et al. (2013) Magnetic Resonance Imaging–Based Three-Dimensional Bone Shape of the Knee Predicts Onset of Knee Osteoarthritis: Data From the Osteoarthritis Initiative. Arthritis & Rheumatism 65: 2048-2058.
5. Brunt LH, Norton JL, Bright JA, Rayfield EJ, Hammond CL (2015) Finite element modelling predicts changes in joint shape and cell behaviour due to loss of muscle strain in jaw development. J Biomech 48: 3112-3122.
6. Roddy KA, Prendergast PJ, Murphy P (2011) Mechanical influences on morphogenesis of the knee joint revealed through morphological, molecular and computational analysis of immobilised embryos. PLoS One 6: e17526.
7. Roddy KA, Kelly GM, van Es MH, Murphy P, Prendergast PJ (2011) Dynamic patterns of mechanical stimulation co-localise with growth and cell proliferation during morphogenesis in the avian embryonic knee joint. J Biomech 44: 143-149.
8. Nowlan NC, Bourdon C, Dumas G, Tajbakhsh S, Prendergast PJ, et al. (2010) Developing bones are differentially affected by compromised skeletal muscle formation. Bone 46: 1275-1285.
9. Murray PD, Drachman DB (1969) The role of movement in the development of joints and related structures: the head and neck in the chick embryo. J Embryol Exp Morphol 22: 349-371.
10. Nowlan NC, Chandaria V, Sharpe J (2014) Immobilized chicks as a model system for early-onset developmental dysplasia of the hip. J Orthop Res 32: 777-785.
11. Mikic B, Johnson TL, Chhabra AB, Schalet BJ, Wong M, et al. (2000) Differential effects of embryonic immobilization on the development of fibrocartilaginous skeletal elements. J Rehabil Res Dev 37: 127-133.
12. Osborne AC, Lamb KJ, Lewthwaite JC, Dowthwaite GP, Pitsillides AA (2002) Short-term rigid and flaccid paralyses diminish growth of embryonic chick limbs and abrogate joint cavity formation but differentially preserve pre-cavitated joints. J Musculoskelet Neuronal Interact 2: 448-456.
13. Rolfe RA, Nowlan NC, Kenny EM, Cormican P, Morris DW, et al. (2014) Identification of mechanosensitive genes during skeletal development: alteration of genes associated with cytoskeletal rearrangement and cell signalling pathways. BMC Genomics 15: 48.
14. Nowlan NC, Dumas G, Tajbakhsh S, Prendergast PJ, Murphy P (2012) Biophysical stimuli induced by passive movements compensate for lack of skeletal muscle during embryonic skeletogenesis. Biomech Model Mechanobiol 11: 207-219.
15. Shwartz Y, Farkas Z, Stern T, Aszodi A, Zelzer E (2012) Muscle contraction controls skeletal morphogenesis through regulation of chondrocyte convergent extension. Dev Biol 370: 154-163.
16. Brunt LH, Skinner REH, Roddy KA, Araujo NM, Rayfield EJ, et al. (2016) Differential effects of altered patterns of movement and strain on joint cell behaviour and skeletal morphogenesis. Osteoarthritis and Cartilage 24: 1940-1950.

549 17. Smith RL, Carter DR, Schurman DJ (2004) Pressure and Shear Differentially Alter Human
550 Articular Chondrocyte Metabolism: A Review. Clinical Orthopaedics and Related
551 Research 427: S89-S95.
552 18. Wong M, Siegrist M, Goodwin K (2003) Cyclic tensile strain and cyclic hydrostatic
553 pressure differentially regulate expression of hypertrophic markers in primary
554 chondrocytes. Bone 33: 685-693.
555 19. Wu Q-q, Zhang Y, Chen Q (2001) Indian hedgehog Is an Essential Component of
556 Mechanotransduction Complex to Stimulate Chondrocyte Proliferation. Journal of
557 Biological Chemistry 276: 35290-35296.
558 20. Burleigh A, Chanalaris A, Gardiner MD, Driscoll C, Boruc O, et al. (2012) Joint
559 immobilization prevents murine osteoarthritis and reveals the highly
560 mechanosensitive nature of protease expression in vivo. Arthritis & Rheumatism 64:
561 2278-2288.
562 21. Intema F, Van Roermund PM, Marijnissen ACA, Cotofana S, Eckstein F, et al. (2011)
563 Tissue structure modification in knee osteoarthritis by use of joint distraction: an
564 open 1-year pilot study. Annals of the Rheumatic Diseases.
565 22. Watt FE, Kennedy DL, Carlisle KE, Freidin AJ, Szydlo RM, et al. (2014) Night-time
566 immobilization of the distal interphalangeal joint reduces pain and extension
567 deformity in hand osteoarthritis. Rheumatology 53: 1142-1149.
568 23. Ando A, Suda H, Hagiwara Y, Onoda Y, Chimoto E, et al. (2011) Reversibility of
569 immobilization-induced articular cartilage degeneration after remobilization in rat
570 knee joints. Tohoku J Exp Med 224: 77-85.
571 24. Bartolomé N, Segarra S, Artieda M, Francino O, Sánchez E, et al. (2015) A Genetic
572 Predictive Model for Canine Hip Dysplasia: Integration of Genome Wide Association
573 Study (GWAS) and Candidate Gene Approaches. PLOS ONE 10: e0122558.
574 25. Vanden Berg-Foels WS, Todhunter RJ, Schwager SJ, Reeves AP (2006) Effect of Early
575 Postnatal Body Weight on Femoral Head Ossification Onset and Hip Osteoarthritis in
576 a Canine Model of Developmental Dysplasia of the Hip. Pediatr Res 60: 549-554.
577 26. Bo N, Peng W, Xinghong P, Ma R (2012) Early Cartilage Degeneration in a Rat
578 Experimental Model of Developmental Dysplasia of the Hip. Connective Tissue
579 Research 53: 513-520.
580 27. Greenhill BJ, Hainau B, Ellis RD, el-Sayed RM (1995) Acetabular changes in an
581 experimental model of developmental dysplasia of the hip (DDH). J Pediatr Orthop
582 15: 789-793.
583 28. Askary A, Mork L, Paul S, He X, Izuhara AK, et al. (2015) Iroquois Proteins Promote
584 Skeletal Joint Formation by Maintaining Chondrocytes in an Immature State. Dev Cell
585 35: 358-365.
586 29. Hayes AJ, Reynolds S, Nowell MA, Meakin LB, Habicher J, et al. (2013) Spinal deformity in
587 aged zebrafish is accompanied by degenerative changes to their vertebrae that
588 resemble osteoarthritis. PLoS One 8: e75787.
589 30. Curado S, Anderson RM, Jungblut B, Mumm J, Schroeter E, et al. (2007) Conditional
590 targeted cell ablation in zebrafish: A new tool for regeneration studies.
591 Developmental Dynamics 236: 1025-1035.
592 31. Hinits Y, Williams VC, Sweetman D, Donn TM, Ma TP, et al. (2011) Defective cranial
593 skeletal development, larval lethality and haploinsufficiency in Myod mutant
594 zebrafish. Dev Biol 358: 102-112.

595 32. Kronenberg HM (2003) Developmental regulation of the growth plate. Nature 423: 332-
596 336.
597 33. Shwartz Y, Blitz E, Zelzer E (2013) One load to rule them all: Mechanical control of the
598 musculoskeletal system in development and aging. Differentiation 86: 104-111.
599 34. Dutton KA, Pauliny A, Lopes SS, Elworthy S, Carney TJ, et al. (2001) Zebrafish colourless
600 encodes sox10 and specifies non-ectomesenchymal neural crest fates. Development
601 128: 4113-4125.
602 35. Li Q, Lau A, Morris TJ, Guo L, Fordyce CB, et al. (2004) A Syntaxin 1, $G\alpha_o$, and N-Type
603 Calcium Channel Complex at a Presynaptic Nerve Terminal: Analysis by Quantitative
604 Immunocolocalization. The Journal of Neuroscience 24: 4070-4081.
605 36. Persson M (1983) The role of movements in the development of sutural and diarthrodial
606 joints tested by long-term paralysis of chick embryos. J Anat 137 (Pt 3): 591-599.
607 37. Eames BF, Amores A, Yan Y-L, Postlethwait JH (2012) Evolution of the osteoblast:
608 skeletogenesis in gar and zebrafish. BMC Evolutionary Biology 12: 27.
609 38. Askary A, Smeeton J, Paul S, Schindler S, Braasch I, et al. (2016) Ancient origin of
610 lubricated joints in bony vertebrates. eLife 5: e16415.
611 39. Chen JW, Galloway JL (2014) The development of zebrafish tendon and ligament
612 progenitors. Development 141: 2035-2045.
613 40. Smeeton J, Askary A, Crump JG (2017) Building and maintaining joints by exquisite local
614 control of cell fate. Wiley Interdisciplinary Reviews: Developmental Biology 6: e245-
615 n/a.
616 41. Hammond CL, Moro E (2012) Using transgenic reporters to visualize bone and cartilage
617 signaling during development in vivo. Front Endocrinol (Lausanne) 3: 91.
618 42. Koyama E, Shibukawa Y, Nagayama M, Sugito H, Young B, et al. (2008) A distinct cohort
619 of progenitor cells participates in synovial joint and articular cartilage formation
620 during mouse limb skeletogenesis. Developmental Biology 316: 62-73.
621 43. Solem RC, Eames BF, Tokita M, Schneider RA (2011) Mesenchymal and mechanical
622 mechanisms of secondary cartilage induction. Developmental Biology 356: 28-39.
623 44. Pollard AS, Charlton BG, Hutchinson JR, Gustafsson T, McGonnell IM, et al. (2017) Limb
624 proportions show developmental plasticity in response to embryo movement.
625 Scientific Reports 7: 41926.
626 45. De R, Zemel A, Safran SA (2007) Dynamics of cell orientation. Nat Phys 3: 655-659.
627 46. McMahon LA, O'Brien FJ, Prendergast PJ (2008) Biomechanics and mechanobiology in
628 osteochondral tissues. Regenerative Medicine 3: 743-759.
629 47. Sharma G, Saxena RK, Mishra P (2007) Differential effects of cyclic and static pressure on
630 biochemical and morphological properties of chondrocytes from articular cartilage.
631 Clinical Biomechanics 22: 248-255.
632 48. Wu Q-q, Chen Q (2000) Mechanoregulation of Chondrocyte Proliferation, Maturation,
633 and Hypertrophy: Ion-Channel Dependent Transduction of Matrix Deformation
634 Signals. Experimental Cell Research 256: 383-391.
635 49. Jacobsen S, Sonne-Holm S (2005) Hip dysplasia: a significant risk factor for the
636 development of hip osteoarthritis. A cross-sectional survey. Rheumatology 44: 211-
637 218.
638 50. Gemberling M, Bailey TJ, Hyde DR, Poss KD (2013) The zebrafish as a model for complex
639 tissue regeneration. Trends in Genetics 29: 611-620.
640 51. Westerfield M (2000) The zebrafish book. A guide for the laboratory use of zebrafish
641 (Danio rerio). Univ. of Oregon Press, Eugene

642 52. Hammond CL, Schulte-Merker S (2009) Two populations of endochondral osteoblasts
643 with differential sensitivity to Hedgehog signalling. Development 136: 3991-4000.
644 53. Dutton JR, Antonellis A, Carney TJ, Rodrigues FS, Pavan WJ, et al. (2008) An
645 evolutionarily conserved intronic region controls the spatiotemporal expression of
646 the transcription factor Sox10. BMC Dev Biol 8: 105.
647 54. Elworthy S, Hargrave M, Knight R, Mebus K, Ingham PW (2008) Expression of multiple
648 slow myosin heavy chain genes reveals a diversity of zebrafish slow twitch muscle
649 fibres with differing requirements for Hedgehog and Prdm1 activity. Development
650 135: 2115-2126.
651 55. Lee RTH, Knapik EW, Thiery JP, Carney TJ (2013) An exclusively mesodermal origin of fin
652 mesenchyme demonstrates that zebrafish trunk neural crest does not generate
653 ectomesenchyme. Development 140: 2923-2932.
654 56. Hatta K, Tsujii H, Omura T (2006) Cell tracking using a photoconvertible fluorescent
655 protein. Nat Protocols 1: 960-967.
656 57. Mitchell RE, Huitema LF, Skinner RE, Brunt LH, Severn C, et al. (2013) New tools for
657 studying osteoarthritis genetics in zebrafish. Osteoarthritis Cartilage 21: 269-278.
658 58. Brunt LH, Begg K, Kague E, Cross S, Hammond CL (2017) Wnt Signalling Controls the
659 Response to Mechanical Loading during Zebrafish Joint Development. bioRxiv.
660 59. Hammer O, Harper DAT, Ryan PD (2001) Paleontological statistics software package for
661 education and data analysis. Paleontologia Electronica 4: 9.
662 60. Edelsbrunner H, Kirkpatrick D, Seidel R (1983) On the shape of a set of points in the
663 plane. IEEE Transactions on Information Theory 29: 551-559.
664 61. Schindelin J, Arganda-Carreras I, Frise E, Kaynig V, Longair M, et al. (2012) Fiji: an open-
665 source platform for biological-image analysis. Nat Meth 9: 676-682.
666 62. Hall BK, Herring SW (1990) Paralysis and growth of the musculoskeletal system in the
667 embryonic chick. J Morphol 206: 45-56.
668 63. Reiser PJ, Stokes BT, Walters PJ (1988) Effects of immobilization on the isometric
669 contractile properties of embryonic avian skeletal muscle. Experimental Neurology
670 99: 59-72.
671 64. Maeda T, Sakabe T, Sunaga A, Sakai K, Rivera Alexander L, et al. (2011) Conversion of
672 Mechanical Force into TGF-β-Mediated Biochemical Signals. Current Biology 21: 933-
673 941.

674

675

676 ***Figure legends***

677 Fig 1. Restoration of muscle contraction is sufficient to drive the recovery of jaw function and
678 shape.

679 Zebrafish expressing Tg(*Col2a1aBAC:mcherry*) were imaged laterally (1,2) and ventrally (3-
680 4) at 5dpf (A-C) and 7 dpf (E-I). Immobilisation and ablation caused joint subluxation
681 (arrows, B1-2, C1-2) and flattening of mandibular symphysis (ms, B3-4, C3-4). The number

682 of mouth openings per 500 frames at 5dpf in anaesthetised larvae, after wash out, and
683 ablated larvae (D) analysed by 2-way anova. 7dpf anaesthetised and ablated larva
684 subdivided by jaw position (F-I). Time course of percentage recovery following varying
685 anaesthesia treatment analysed using Kruskal-Wallis test (K). (a) p=0.009 “24hrs 3-4” vs “48
686 hrs”, (b) p=0.008 “24 hrs 3-4” vs “24 hrs 4-5”, (c) p=0.049 “24hrs 3-4” vs “56 hrs” and (d)
687 p=0.002 “24hrs 3-4” vs “56 hrs”. m; Meckel’s cartilage, ch; ceratohyal, pq; palatoquadrate,
688 RAP; retro-articular process.

689 Fig 2. Shape cannot be used to predict recovery in anaesthetised or ablated larvae however
690 restored movement significantly altered the shape of the Meckel’s cartilage by 7dpf.

691 Graphic representation of results of npManova (B, C) of 2D outline of
692 Tg(*Col2a1aBac:mcherry*) larvae (A). Principal component analysis of 5 (D) and 7dpf (E)
693 treatment grouped by colour and subdivided by jaw position at 7dpf. Selected joint examples
694 arranged according to PC1 and 2 at 5 dpf (F) and 7dpf (G) showing the increasing thickness
695 of the MC (double arrow), overlapping joint shape (arrow) and altered curvature of the
696 cartilage (PC2, double arrow).

697 Fig 3. Chondrocyte maturation is less affected in the mandibular symphysis and jaw joint of
698 larvae that recover.

699 Confocal images of the mandibular symphysis of 5dpf and 7dpf control, myod-/-,
700 anaesthetised and ablated zebrafish cartilage visualised using the Tg(Col2a1aBAC:mcherry)
701 transgenic line (A-J). Confocal image of a representative jaw joint (O). Cell circularity (K, L)
702 and cell area (M, N, P, Q) of 10 cells, outlined in red, between the insertion of the
703 intermandibularis muscle (n=6 per condition) (A-N) and below intercalation in the joint (O).
704 1.00 represents a perfect circle.

705 Fig 4. Restored movement drives the restoration of the joint line.

706 Ventrally imaged zebrafish expressing Tg*(Col2a1aBAC:mcherry)* and *Tg(-*
707 *4725sox10:GFP)*^{ba4} at 3, 5 and 7dpf and laterally at 3 and 5dpf. High magnification confocal

708 images of the joint line of 5dpf (B) and 7dpf (C). Ablated and anaesthetised larvae which
709 were subdivided by their jaw position at 7dpf. Joint volume (D, E) derived from the "product
710 of the difference of the mean" (PDM) of the joint (white box). JL; joint line, Syml; mandibular
711 symphysis PQ; palatoquadrate, mc; Meckel's cartilage, Ch; ceratohyal.

712 Fig 5. Cell proliferation and migration is differentially regulated in zebrafish that recover
713 relative to those that remain subluxed.

714 BrdU incorporation (green) between 5-7dpf (A). Arrows show BrdU+ cells within the
715 cartilage. Arrowhead shows BrdU+ incorporation outside the cartilage. Cells expressing
716 Tg(Sox10:GAL4-VP16) and Tg(UAS:Kaede) are green until photoconverted. Red
717 photoconverted cells located on the medial or lateral sides of the joint at 5dpf (left panels),
718 reimaged at 7dpf (middle) with detail of photoconverted cells (right). Arrowhead indicates
719 migration, p indicates proliferation. Number BrdU+ cells on the medial and lateral side of the
720 joint in control, anaesthetised recovered and subluxed zebrafish. Fold change in total area of
721 cells (red outline in B) expressing photoconverted red kaede in control, anaesthetised
722 recovered and subluxed. The impact of side and treatment on BrdU+ counts and Kaede
723 growth analysed by MANOVA.

724 Fig 6. Recovery restores joint associated structures.

725 Confocal images of control and anaesthetised TgBAC(Col10a1a:Citrine)^{hu7050} and
726 Tg*(Col2a1aBAC:mcherry)* were imaged ventrally at 5dfp (A-B'') and again at 7dpf (A-G''). At
727 7dpf they were split into recovered and subluxed by jaw position. Detail images of RAP (')
728 and RAP rotated approximately 90° (''). Counts of ColX expressing osteoblasts located at the
729 RAP (arrows in detail images) at 5dpf (C) and 7dpf (H). Width of the Interoperculomandibular
730 ligament (IOM), measured at 3 sites along the ligament at 5dpf (D) and 7dpf (I). Counts of
731 BrdU incorporation into the IOM between 5dpf and 7dpf, prepared within 40μm of its
732 insertion into the RAP in control and anaesthetised larvae split by jaw position at 7dpf (J-K).
733 Analysed by Anova.

734 Fig 7. Finite element (FE) analysis reveals distinct differences between the patterns of
735 biophysical stimuli

736 FE model simulating jaw displacement during closure in models of a 5 dpf control and anaesthetised
737 larvae that recover (B) or remain subluxed (C). Displacement is shown as the block colour model
738 relative to the semi-transparaent model of the jaw original position, with the direction of motion
739 indicated as an arrow. Finite element models of maximum principal strain created from confocal
740 stacks of 5 dpf control (D,G, J) and anaesthetised larvae that recovered (E,H, K) or remained
741 subluxed (F,I,L) during closure (D-I) and opening (J-L). Each panel shows a ventral view, enlarged
742 image of the joint (Jj) and mandibular symphysis (MS). Strain was elevated at the symphysis (green
743 arrowhead), RAP (red arrow) and on the lateral side of the joint (black arrow heads) (D-F, J-L). The
744 orientation and magnitude of the strains are indicated by the direction, size and colour of arrows in the
745 plane through the mandibular symphysis (G-I). Graph of the average absolute maximum principal
746 strain during opening and closure (N), extracted from 10 elements on the medial and lateral side of
747 the joint in a plane located at the midpoint of the joint (redline M).

748 *Supplementary Figures:*

749 S1 Fig. Muscle repair post ablation. *Smyhc:egfp* and *Col2a1:mcherry* transgenic zebrafish
750 were bilaterally ablated at 3dpf and imaged at 4dpf and 5dpf. Yellow arrowhead indicate
751 ablation site and repairing muscle.

752 S2 Fig. Cell orientations on the medial (A, green cells) and lateral (A, red cells) in wild type,
753 anaesthetised recovered and subluxed and myod-/- and bilaterally ablated zebrafish jaw
754 joints. Orientation angle, calculated from the longest axis of the cell (A, insert) of
755 chondrocytes 5dpf (B) and 7dpf (C) zebrafish in the Meckel's cartilage element of the joint,
756 plotted on circular histograms (rose plots), where 0° lies on the medial side of the joint and
757 180° at the lateral side of the joint. n=6 joints per experimental condition (1 or 2 refers to
758 number of joints per blue wedge). Histogram bins equal 20°. The red line marks mean
759 orientation and the green line marks the 95% confidence interval and analysed by MANOVA.

760 S3 Fig. Differential expression of *Sox10:gfp* and *Col2a1:mcherry* is lost in the joints of Myod-
761 /- zebrafish. The intensity of product of the difference of the mean (PDM) between *Sox10:gfp*
762 and *Col2a1:mcherry* double transgenic in control, anaesthetise recovered and subluxed,
763 Myod mutants and double ablated zebra fish.

764 S4 Fig. Muscle fibres numbers reduced after ablation. Confocal images of control (A,C,E)
765 and adductor mandibularis (AM) ablated (B,D,F) transgenic *smyhc;EGFP* (A-B) zebrafish
766 following immunohistochemistry for total Myosin (C-D) show significant reduction in the
767 reduction in the number of fibres (G). Percentage of Fish divided by the success of ablation
768 (H). Arrowhead indicates adductor mandibularis.

769 S5 Fig. Building Finite element (FE) models.

770 3D surfaces were generated from confocal images of 5dpf *Smyhc:egfp* and *Col2a1:mcherry*
771 control (A) and anaesthetised larvae (C,E) were used to generate FE models (O-Q).
772 Anaesthetised larvae were subdivide by their jaw position at 7dpf (C, E). By 7dpf the
773 recovered larva (F) was significantly different in shape to the subluxed (D). Sections through
774 the jaw joint (J,K,N indicated by white line) show a continuous interzone in the joint (J', N',
775 arrowhead) and mandibular symphysis (MS) (G, I, arrowhead) of controls and the recovered
776 larva at 5dpf but not the subluxed. A spring modelled the Interoperculomandibular ligament
777 (IOM) between the retro articular process (RAP) and Hyod bone (P-R, yellow line). 50% of
778 maximum muscle loads (measured in Newtons (N)) were applied at the origin and insertion of the
779 muscle The adductor mandibulae **(**AM) (O',P',Q', blues line) was applied to model mouth closure. To
780 capture the wider insertion of the intermandibularis (IM) and protractor hyoideus (PH) (O) the forces
781 were applied across 10 nodes to model of mouth opening (O"-Q"). White dots indicate the area of
782 applied constraints in either the x,y, or z orientation (O).

783

784 S6 Fig. Finite element (FE) models of minimum principal strain (Emin).

785 Finite element models of minimum principal strain (compressive) created from confocal stacks of 5 dpf
786 control (A,D) and anaesthetised larvae that recovered (B, E) or remained subluxed (C,F) during
787 closure (A-C) and opening (D-F). Each panel shows a ventral view, enlarged image of the joint (Jj)
788 and mandibular symphysis (MS). Strain was elevated RAP (red arrow).

789

790 S1 Video. Movie of jaw movement at 5dpf control larvae expressing *Col2a1:mcherry.*

791 S2 Video. Movie of jaw movement at 5dpf anaesthetised larvae expressing *Col2a1:mcherry*.

792 S3 Video. Movie of jaw movement at 5dpf in double ablated larvae expressing
793 *Col2a1:mcherry*

794

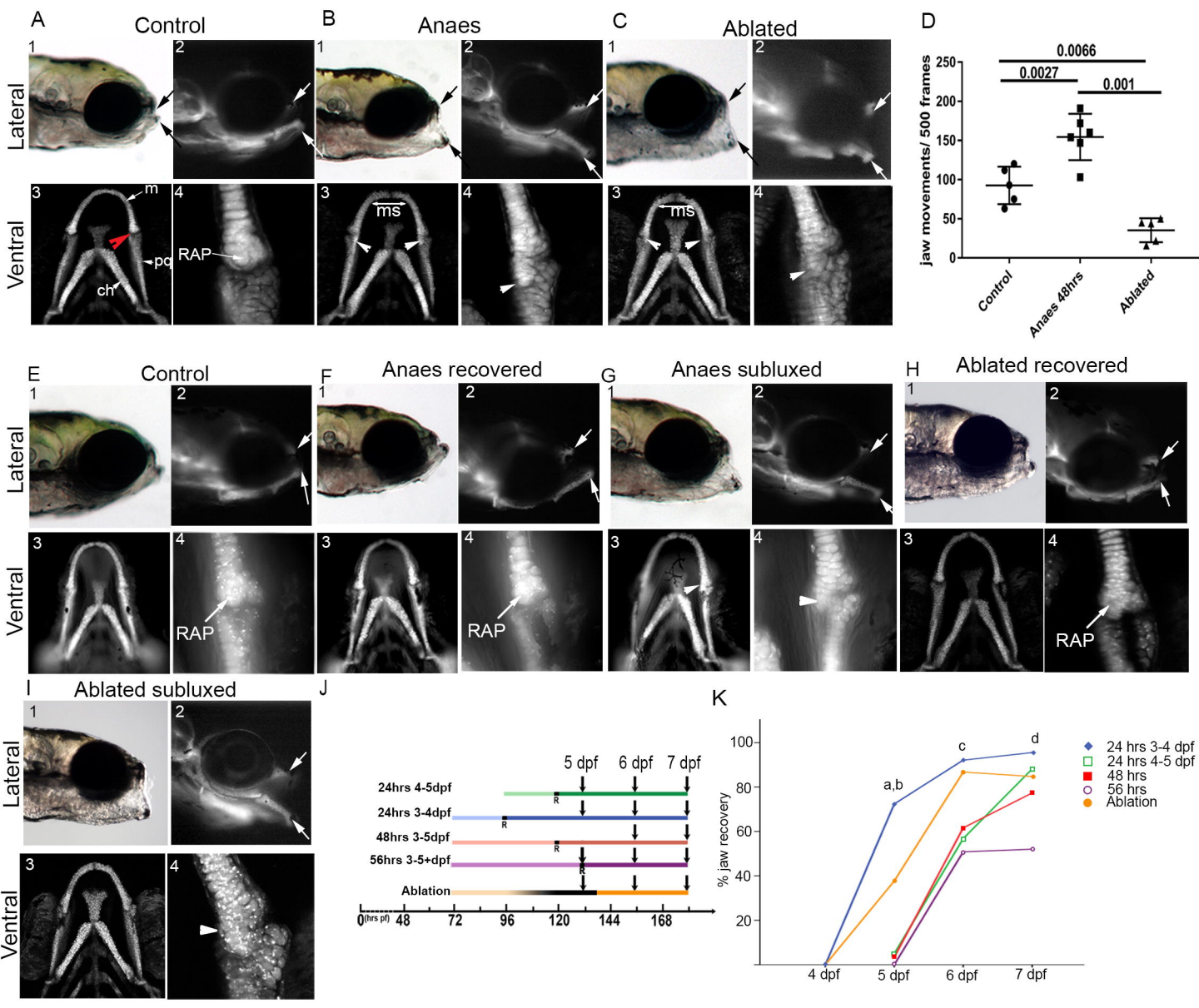
A
Control
B
Anaes
C
Ablated
D
Lateral
Ventral
m
pq
ch
RAP
ms
0.0066
0.0027
0.001
jaw movements/ 500 frames
Control
Anaes 48hrs
Ablated
E
Control
F
Anaes recovered
G
Anaes subluxed
H
Ablated recovered
I
Ablated subluxed
J
5 dpf
6 dpf
7 dpf
24hrs 4-5dpf
24hrs 3-4dpf
48hrs 3-5dpf
56hrs 3-5+dpf
Ablation
0(hrs pf)
48
72
96
120
144
168
K
% jaw recovery
a,b
c
d
24 hrs 3-4 dpf
24 hrs 4-5 dpf
48 hrs
56 hrs
Ablation
4 dpf
5 dpf
6 dpf
7 dpf

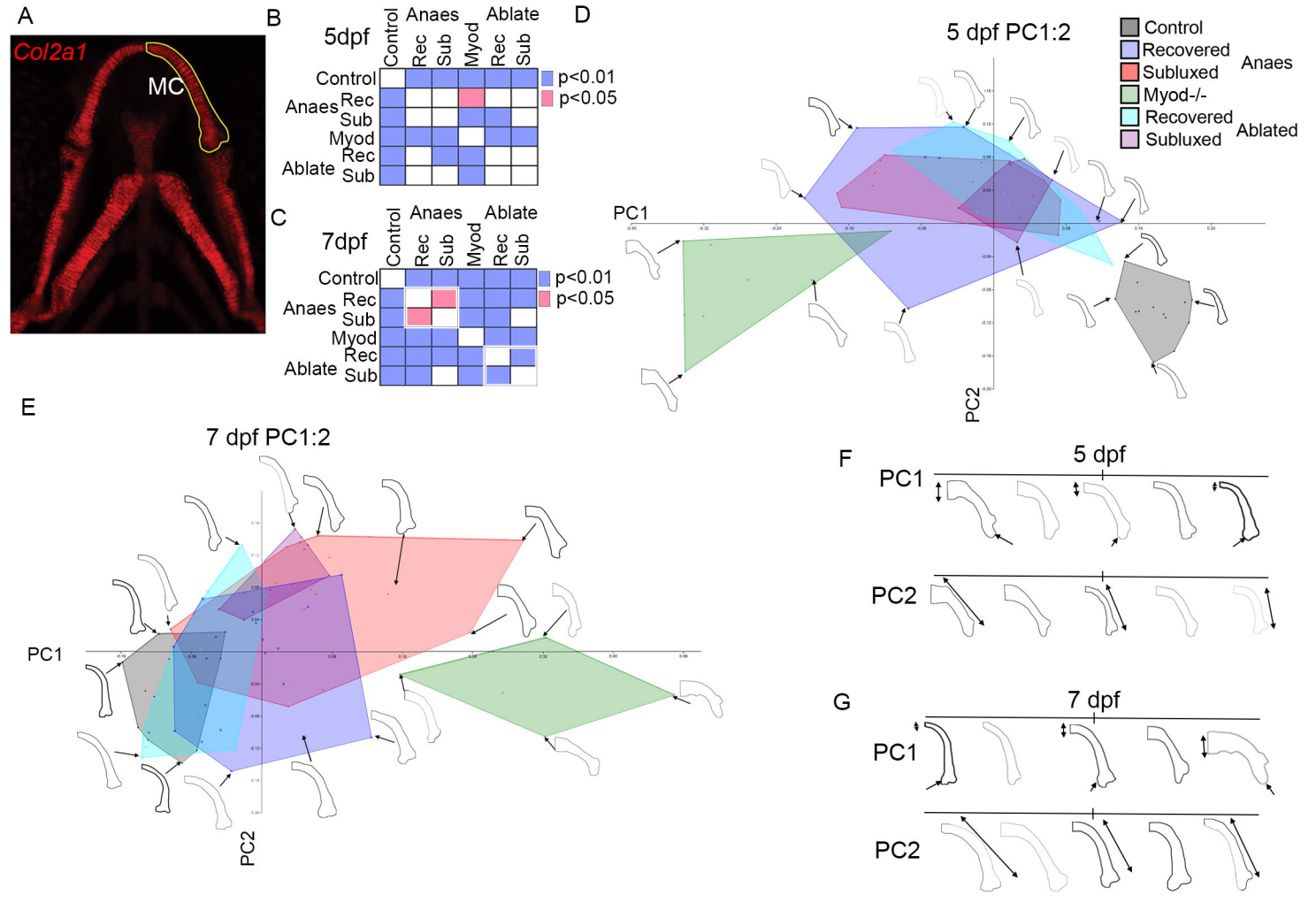
A
Col2a1
MC
B
5dpf
Control
Anaes
Ablate
Rec
Sub
Myod
p<0.01
p<0.05
C
7dpf
D
5 dpf PC1:2
Control
Recovered
Subluxed
Myod-/-
Recovered
Subluxed
Anaes
Ablated
PC1
PC2
E
7 dpf PC1:2
F
5 dpf
G
7 dpf

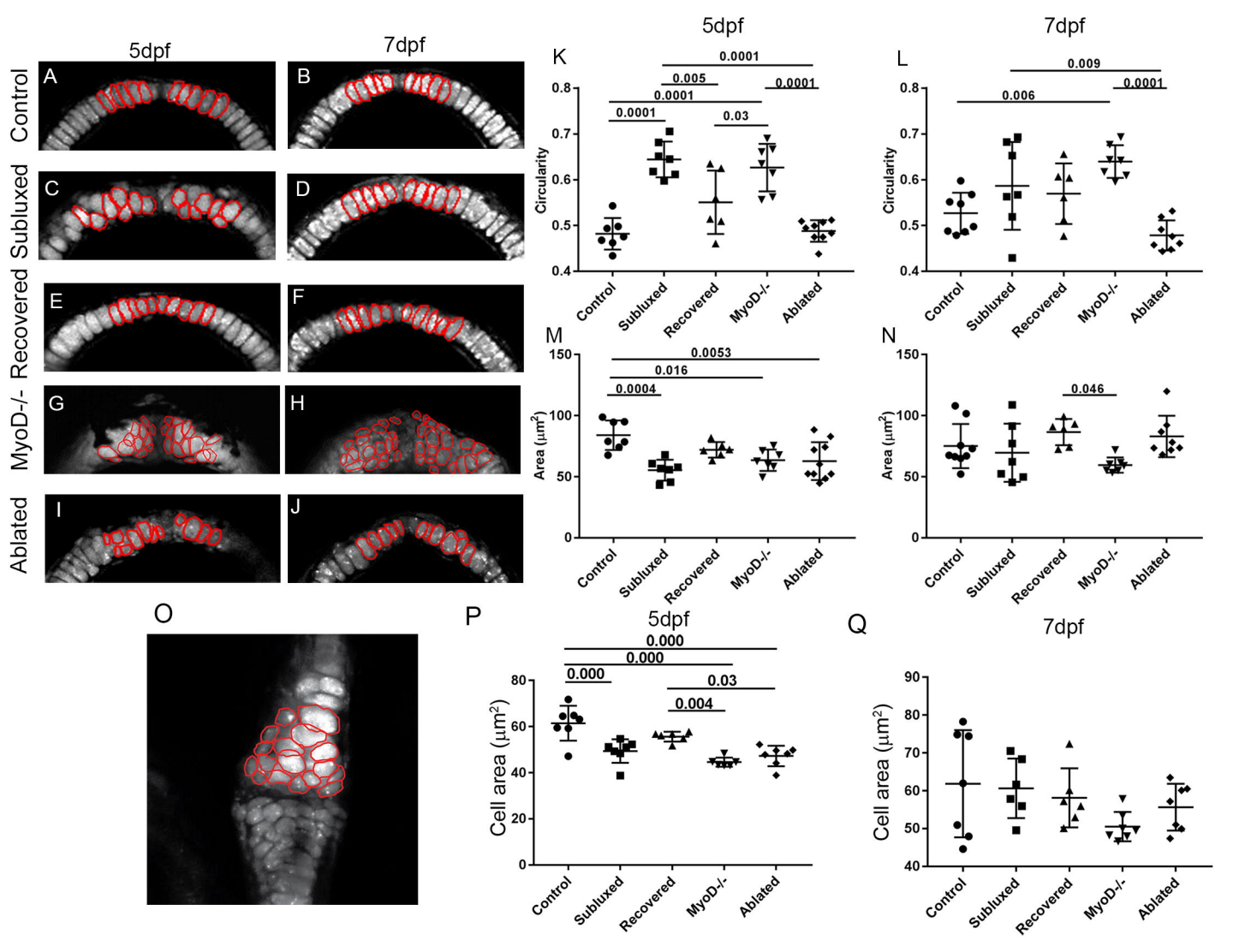
5dpf
7dpf
Control
Subluxed
Recovered
MyoD-/-
Ablated
A
B
C
D
E
F
G
H
I
J
K
L
M
N
O
P
Q
Circularity
Area (μm²)
Cell area (μm²)
0.0001
0.005
0.0001
0.0001
0.03
0.009
0.0001
0.006
0.0053
0.016
0.0004
0.046
0.000
0.000
0.03
0.004

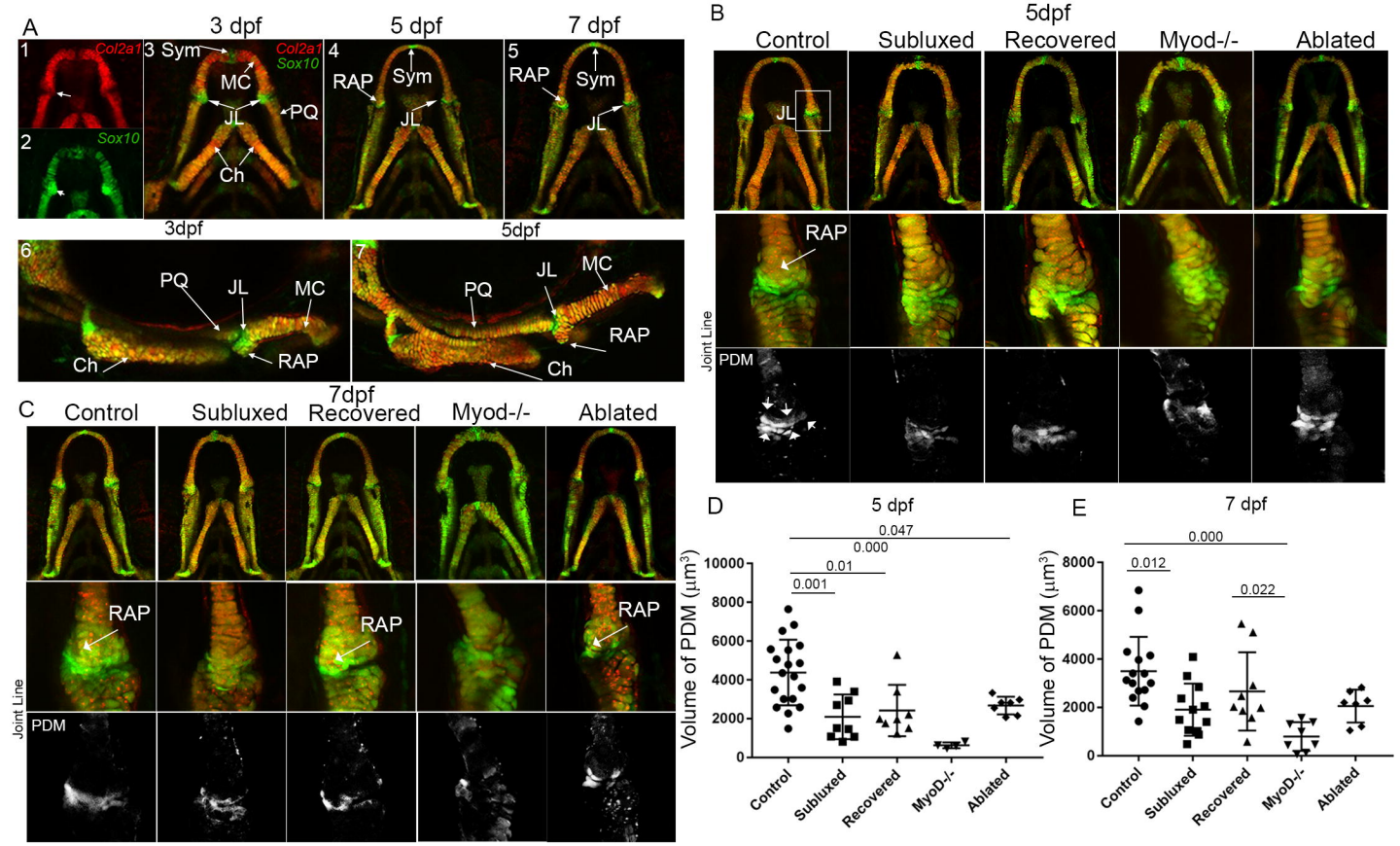
A
3 dpf
5 dpf
7 dpf
1
Col2a1
2
Sox10
3 Sym
Col2a1
Sox10
MC
JL
PQ
Ch
4
RAP
Sym
JL
5
RAP
Sym
JL
3dpf
5dpf
6
PQ
JL
MC
Ch
RAP
7
PQ
JL
MC
RAP
Ch
B
5dpf
Control
Subluxed
Recovered
Myod-/-
Ablated
JL
RAP
Joint Line
PDM
C
7dpf
Control
Subluxed
Recovered
Myod-/-
Ablated
RAP
RAP
RAP
Joint Line
PDM
D
5 dpf
0.047
0.000
0.01
0.001
Volume of PDM (µm3)
10000
8000
6000
4000
2000
0
Control
Subluxed
Recovered
MyoD-/-
Ablated
E
7 dpf
0.000
0.012
0.022
Volume of PDM (µm3)
8000
6000
4000
2000
0
Control
Subluxed
Recovered
MyoD-/-
Ablated

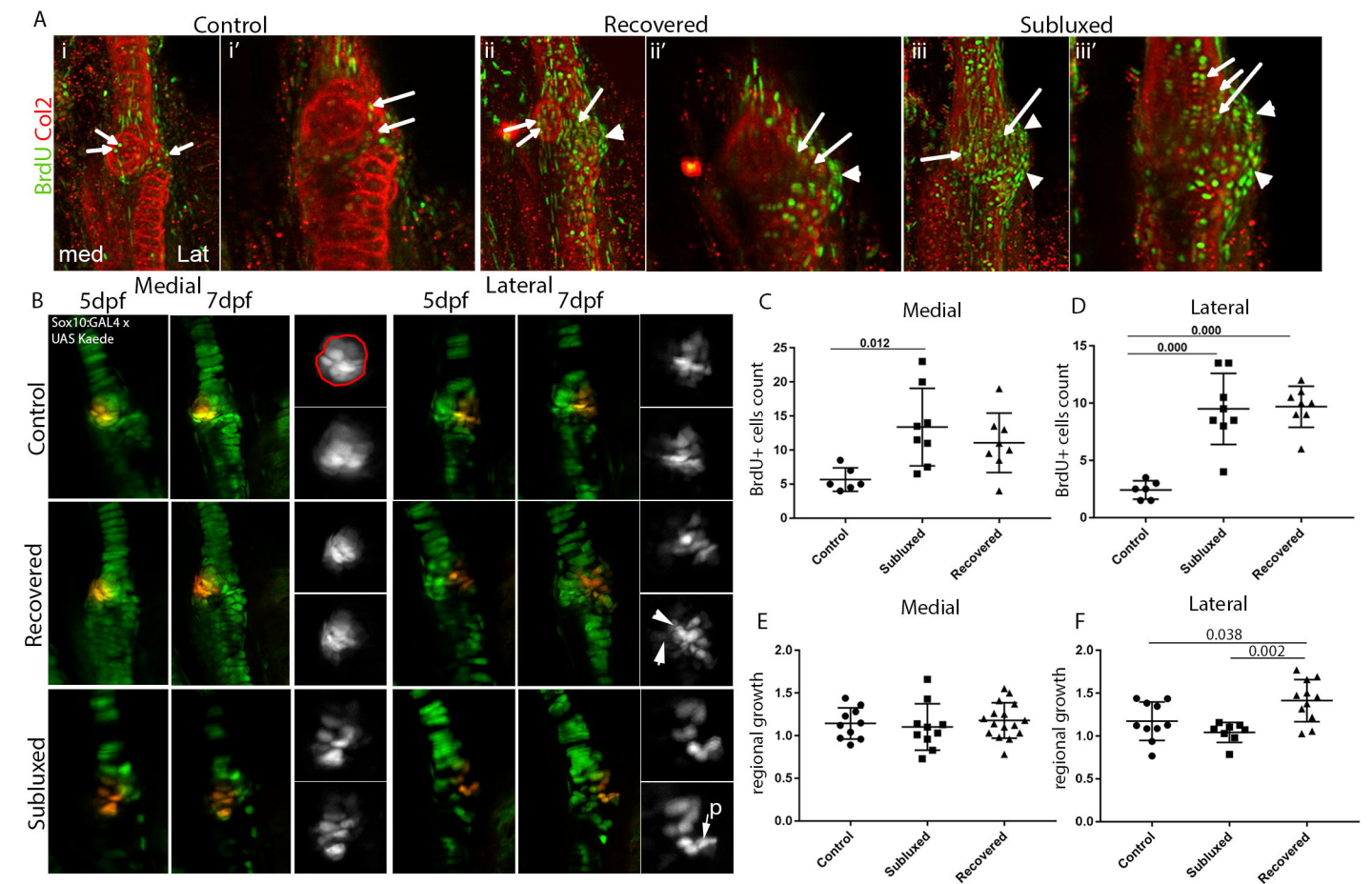
A
Control
Recovered
Subluxed
i
i'
ii
ii'
iii
iii'
BrdU Col2
med
Lat
B
Medial
Lateral
5dpf
7dpf
5dpf
7dpf
Sox10:GAL4 x
UAS Kaede
Control
Recovered
Subluxed
p
C
Medial
BrdU+ cells count
0.012
Control
Subluxed
Recovered
D
Lateral
BrdU+ cells count
0.000
0.000
Control
Subluxed
Recovered
E
Medial
regional growth
Control
Subluxed
Recovered
F
Lateral
regional growth
0.038
0.002
Control
Subluxed
Recovered

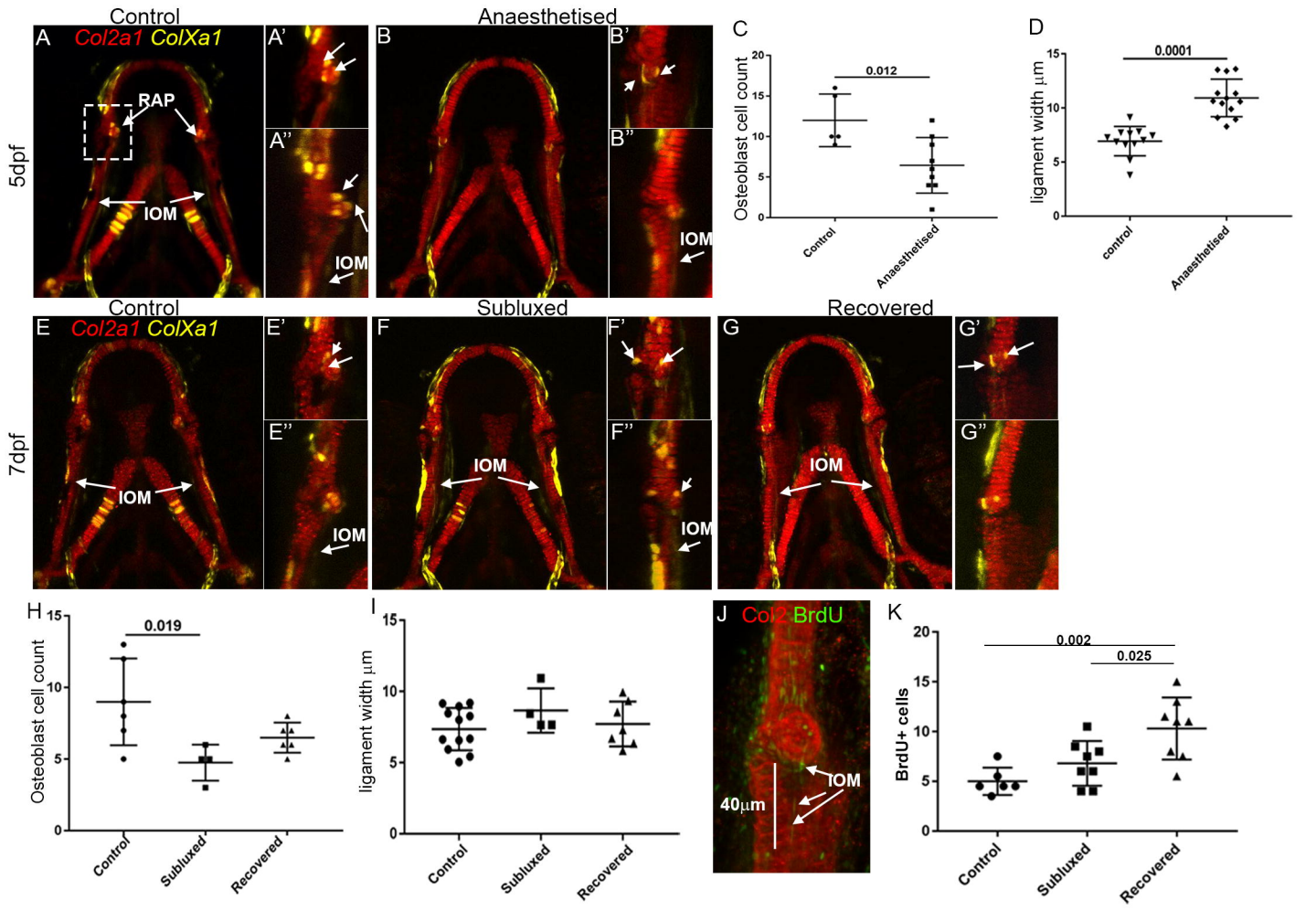
Control
Anaesthetised
5dpf
A
Col2a1 ColXa1
RAP
IOM
A'
A''
B
B'
B''
IOM
C
Osteoblast cell count
0.012
Control
Anaesthetised
D
ligament width µm
0.0001
control
Anaesthetised
Control
Subluxed
Recovered
7dpf
E
E'
E''
F
F'
F''
G
G'
G''
H
Osteoblast cell count
0.019
Control
Subluxed
Recovered
I
ligament width µm
J
Col2 BrdU
40µm
K
BrdU+ cells
0.002
0.025

A
Control
B
Recovered
C
Subluxed
μm
100
50
0
D
E
F
MS
MC
Jj
Ch
Pq
E Max P
(μ strain)
7000
3500
0
Close
G
H
I
E Max P
(μ strain)
10000
5000
0
2000
1000
MS
J
K
L
Open
M
MC
medial
interzone
Lateral
PQ
N
unloaded
Open
Close
40
0
-40
-80
-120
tension
compression
Absolute E Max P (μ strain)
Medial
Control
Recovered
Subluxed
Lateral
Control
Recovered
Subluxed